A Tutorial on Modeling Sensory Compound Action Potentials

Gerald Fischer

UMIT TIROL - Private University For Health Sciences and Health Technology

Version 1.0.b, October 2024

Contents

1. Motivation and Concept

This document reaches out for students, which are in an early phase of a biomedical engineering, medical physics, or neuroscience course. It aims to teach basic insight into the genesis of bioelectric signals.

Neuropotentials are in widespread diagnostic use. While being generated by cellular electric activity, clinical settings access signals by macroscopic electrodes, which are mostly located on the body surface. Figure 1 illustrates significant changes in signal properties when moving from a microscopic level to a macroscopic level. A vast body of basic literature exists describing the genesis of a cellular action potentials which reflects activity across the membrane of a single cell (see, e.g., description of the Hodgkin-Huxley model in [1]). However, macroscopic (body surface) electrodes access activity from a large plurality of cells. This activity gets reflected by potential gradients in the extracellular space being accessible by macroscopic electrodes. Notably, on it's way from the cell-membrane to the electrode the signal undergoes remarkable changes in morphology, amplitude and duration. The biophysical effects underlying these diagnostically important signal properties appear being poorly investigated in basic literature.

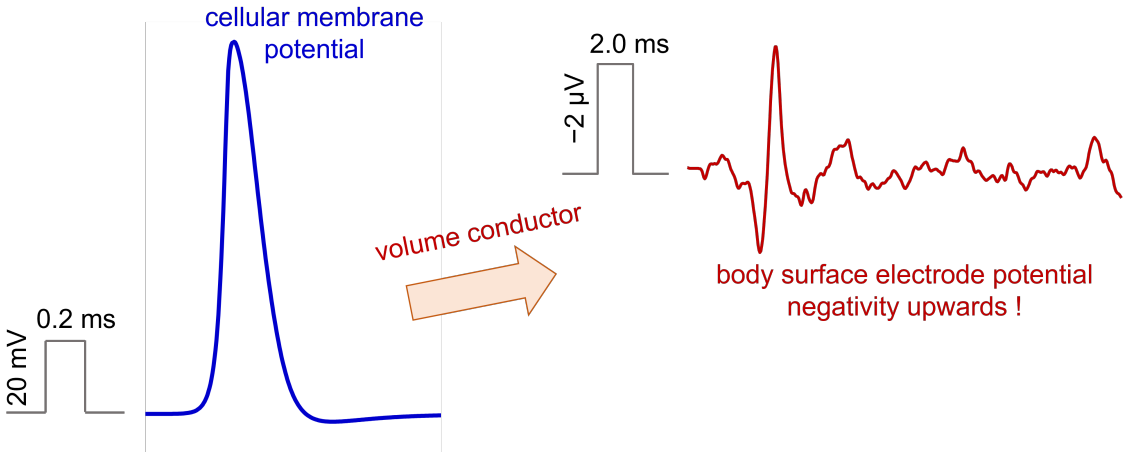

Figure 1: Comparison of a membrane action potential (left, simulated data from [2]) with a sensory compound action potential (CAP) recorded by a body surface electrode (right, experimental data). Calibration pulses indicate scales. Notably, body surface potential amplitude is four orders of magnitude smaller as compared to the membrane potential. Width is increased by about an order of magnitude on the body surface. Following clinical standards negativity is plotted upwards. Thus, also signal morphology appears significantly altered displaying a dominant negativity and a smaller initial positive deflection. Visible background noise is superimposed on the recordings of only a few µV amplitude.

The potential lack of basic literature on the genesis of macroscopic neuropotentials, might be explained by the fact that computation of extracellular potentials in a volume conductor (i.e., a body of a human or an animal) requires the solution of a three dimensional boundary value problem in a complex anatomy. The solution for the potential-field is often obtained using software (i.e., numerical methods like the finite element method). However, such software tools behave like a kind of "black-box" hampering the straight forward perception of relevant biophysical effects.

This tutorial aims for overcoming these limitations by investigating an example which requires only closed dipole-formulas for field computation. Thus, the phenomena underlying the genesis of macroscopic biosignals can be expressed by – hopefully – readable formulas. Sensory compound action potentials (CAPs) are chosen as an example, as the orientation of nerve fibers being (essentially) parallel to the skin, eases the development of dipole models.

This tutorial is organized as follows: it aims to provide a structured treatment, such that readers can follow signal genesis it in a step-by-step fashion. For those who want to dig deeper additional information is provided in footnotes and Appendices.

2. Sensory CAP Model – Time Domain

The model described in this tutorial is a simplified version of a half-space model described in [2]. The scope is to provide a model that explains signal morphology, width, and allows for estimating typical amplitudes.

2.1. Background

A peripheral nerve is a longitudinal neural structure guiding electrical pulses in the body. Sensory nerve fibers guide pulses from peripheral receptors towards the brain (afferent conduction; e.g., the sensation of touching an object). When clinically investigating the function of sensory fibers, a peripheral nerve may be electrically stimulated in a distal location. The response to this stimulation is reflected by a sensory CAP and measured in a more proximal location. An example is shown in Figure 2. The time required for conducting the pulse from the stimulation site to the recording site (in combination with the physical distance of the two sites) allows for computing nerve conduction velocity – a diagnostically relevant parameter. Normal nerve conduction velocity in humans (and mammalians) is in the order of $45\,\mathrm{m\,s^{-1}}$ to $75\,\mathrm{m\,s^{-1}}$, thus, allowing to transmit pulses across the body within a few hundreds of a second [1].

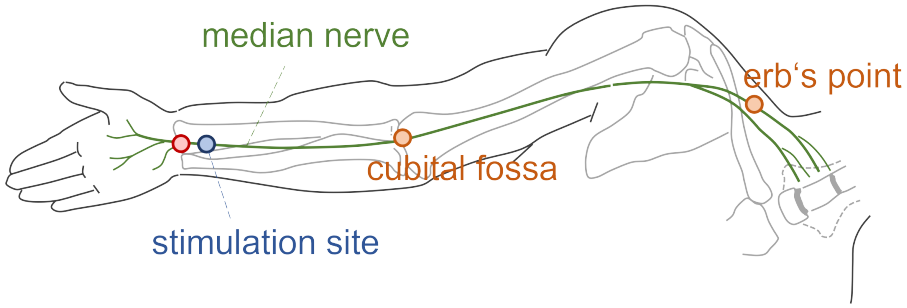

Figure 2: Concept for the measurement of sensory CAPs for the median nerve (i.e., a peripheral nerve). The nerve is stimulated by a cathodic electrode (blue) at the wrist. The CAP can be picked up by an electrode at the cubital fossa (elbow bend) and/or at erb's point (crossing of the nerve with the clavicle). At these two locations the nerve passes relatively close to the body surface.

[1] $75\,\mathrm{m\,s^{-1}}$ correspond to $270\,\mathrm{km\,h^{-1}}$, which is the speed of a race car.

Motoric peripheral nerve fibers guide pulses from the central nervous system to the muscles (motoric function). When stimulating peripheral nerves the motoric responses can be captured by electrodes placed close to the distal muscles. These motoric CAPs are dominated by muscular activity. Therefore, modeling of motoric CAPs requires dedicated models which are not (yet) included in this tutorial.

2.2. Half-Space Model - Overview

Peripheral nerves are composed from long, narrow parallel filaments named **axons**. An axon is that portion of each single neuron (i.e., single nerve cell) which transmits electric pulses over a long distance. In humans, axons of peripheral neurons can extend over a length of up to one meter while their thickness is only in the order of roughly 10 µm. The intracellular space of each axon is surrounded by a membrane of cylindrical shape which controls exchange of ions between the intracellular and extracellular spaces. Below, some important membrane phenomena are briefly reviewed with the scope to model the most important phenomena for computation of body surface potentials. A more complete treatment of membrane ionic current models can be found in literature (e.g., [1]).

A longitudinal peripheral nerve may be modeled by an elongated cylindrical structure in a conducting half-space (Figure 3 a). The nerve contains a plurality (some hundred) of axons. The dashed line in the Figure represents an axon at the center of the nerve. This center is located at a depth s. We aim for computing the CAP in an observation electrode e at the body surface. For convenience, the origin of the coordinate system was located at the electrode.

The potential difference across the membrane (defined as intracelluar minus extracellular potential) is called membrane potential or membrane voltage V_m. Upon activation, a neuron responds with a typical time course (membrane action potential). Figure 3 b) depicts the response of a mammalian sensory axon to stimulation. At rest (i.e., ahead of activation and after an activation cycle) axons generate a constant resting potential of approximately $-70\,\mathrm{mV}$ ("intracellular space is negative at rest"). When activated, the membrane potential increases quickly (about a tenth of a ms) to a maximal value which is approximately 100 mV above the resting value. Then the potential returns to the resting potential. Thus, axonal activation is reflected by a typical action potential containing a depolarization phase ("rise") and repolarization phase ("fall"). We may model this behavior by a linear rise and a linear fall segment. For convenience we define time scale such that time zero is in the middle between the centers of the two linear segments. Therefore, the centers of de- and repolarization are shifted by $\mp\tau$ in time.

The action potential propagates along the axon (Figure 3 c) with a conduction velocity v. Thus, we obtain $V_m(x) = V_m(-vt)$ (see [2]). The de- and repolarization segments generate membrane potential gradients along the axon, which in turn drive currents. Thus, a depolarization dipole and a repolarization dipole of opposite orientation are generated.

2.3. Body Surface Potential of a Single Axon

Axonal Dipole Moments: The strength of the dipole (i.e., the dipole moment) is determined by the product of the impressed dipole current I_D and the length ΔL. A focal dipole model is used for computing the potential on the body surface (i.e., in a location relatively far from the

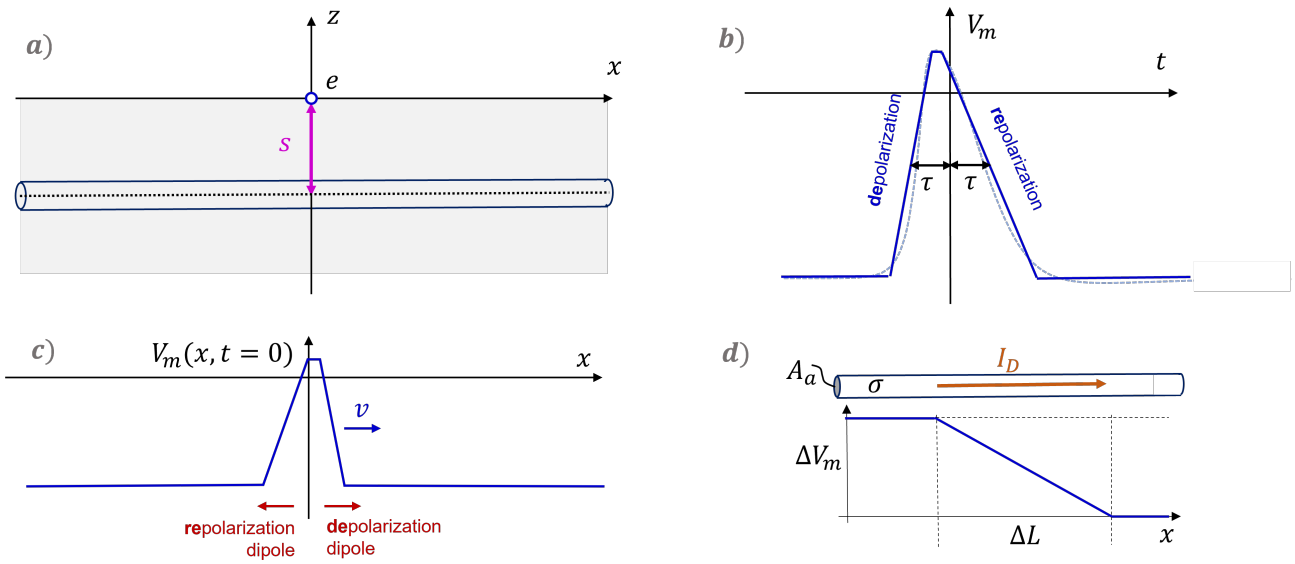

Figure 3: *a)* Model of a longitudinal neural tract in a conducting half-space (depth s, observation electrode e). *b)* Action potential in the time domain. The narrow dashed line depicts simulated data from [2] which is approximated by a piece-wise linear function (full line). *c)* Propagation of an action potential along an axon translates the activation cycle in the time domain into a spatial source pattern. This source pattern can modeled by two dipoles of opposite orientation reflecting de- and repolarization. *d)* Within an axon the potential gradient $-{}^{\Delta V_m}/_{\Delta L}$ drives an impressed current I_D in a segment of length ΔL (dipole source.)

dipole [1]) [2] . The product of the impressed current I_D and the length ΔL defines the dipole moment p_a. Here, I_D is obtained from the product of the membrane potential gradient ${}^{\Delta V_m}/_{\Delta L}$ with the intracellular conductivtiy σ and the axonal cross section A_a. We obtain therefore

$$p_a = \sigma \Delta V_m A_a. \tag{1}$$

Importantly, ΔL gets cancelled in the formula and the dipole moment is, thus, independend of ΔL. Therefore, the de- and repolarisation dipoles have exactly the same magnitude (but opposite orientation) as all remaining parameters are identical. Table 1 lists the parameters used in this tutorial.

Thus, we obtain two dipoles of exactly same strength but opposite orientation. This is called a quadrupole pattern (plus, minus, minus, plus). The CAP is composed by the sum of hundreds or thousands of potentials generated by the individual axons of a nerve. Thus, we will first consider an individual axon potential and will then superimpose potentials. We first consider the potential generated by a single propagating dipole.

Moving Dipole Potential: A dipole traveling along an axon can be described as a moving source point x. Thus, it is of advantage to provide formulas such, that the potential at the

[2] In Neuroscience the term far field is in use with two slightly different meanings. a) For field computation problems far field models allow for simplification of formulas (as in this tutorial). b) In clinical investigations far field potentials are potentials, which are generated by a source being relatively distant from the site of the investigation. For example, an electrode on a shoulder may pick up a brainstem potential.

Table 1: Parameters for the Half-Space Model.

parameter	symbol	value
axon		
membrane potential amplitude	ΔV_m	$100\,\mathrm{mV}$
axonal crosssection	A_a	$100\,\mu\mathrm{m}^2$
intracellular conductivity	σ	$2.0\,\mathrm{S\,m^{-1}}$
conduction velocity	v	$60\,\mathrm{m\,s^{-1}}$
action potential time constant	τ	$0.13\,\mathrm{ms}$
nerve and volume conductor		
number of axons	N	600
bulk conductivity	κ	$0.2\,\mathrm{S\,m^{-1}}$
depth	s	$12\,\mathrm{mm}$

Appendix A reviews the chosen values.

electrode becomes a function of x.

$$\varphi_p(x) = -\frac{p_a}{2\pi\kappa}\frac{x}{(x^2+s^2)^{\frac{3}{2}}}. \tag{2}$$

Here, s is the depth of the neural pathway in the tissue and κ is an average passive conductivity of the tissue surrounding the axon. The open access supplement of [2] provides a derivation of eq. (2). The minus on the right hand side reflects that a variable source point is considered while the field point is fixed (electrode at the origin). For a dipole propagating with a conduction velocity v along the axon, the actual source point is $x = vt$ (thus, at $t = 0$ the dipole passes underneath the observation electrode). We obtain the dipole potential $\varphi_p(t)$ as a function of time

$$\varphi_p(t) = -\frac{p_a}{2\pi\kappa}\frac{vt}{\left[v^2t^2+s^2\right]^{\frac{3}{2}}}. \tag{3}$$

The top left panel in Figure 4 depicts $\varphi_p(t)$ obtained using the parameters defined in Table 1.

Axonal Action Potential: The potential of two dipoles of opposite polarity and temporal displacement $+\tau$ and $-\tau$ is obtained from

$$\varphi_a(t) = \varphi_p(t-\tau) - \varphi_p(t+\tau) = [\delta(t-\tau) - \delta(t+\tau)] * \varphi_p(t). \tag{4}$$

Notably, the time shift of two dipoles of opposite amplitude can be formally expressed by the convolution of two Dirac pulses of opposite sign with $\varphi_p(t)$. In chapter 2.4 we shall take advantage of this observation. Substituting now eq. (3) into (4) we obtain for the axon potential

$$\varphi_a(t) = -\frac{p_a}{2\pi\kappa}\left\{\frac{v(t+\tau)}{\left[v^2(t+\tau)^2+s^2\right]^{\frac{3}{2}}} - \frac{v(t-\tau)}{\left[v^2(t-\tau)^2+s^2\right]^{\frac{3}{2}}}\right\}. \tag{5}$$

The right panel in Figure 4 depicts the axonal potential obtained using the parameters defined in 1. The axonal body surface potential displays a tri-phasic morphology reflecting the underlying quadrupole pattern. The dominating negative peak corresponds to the two negative poles

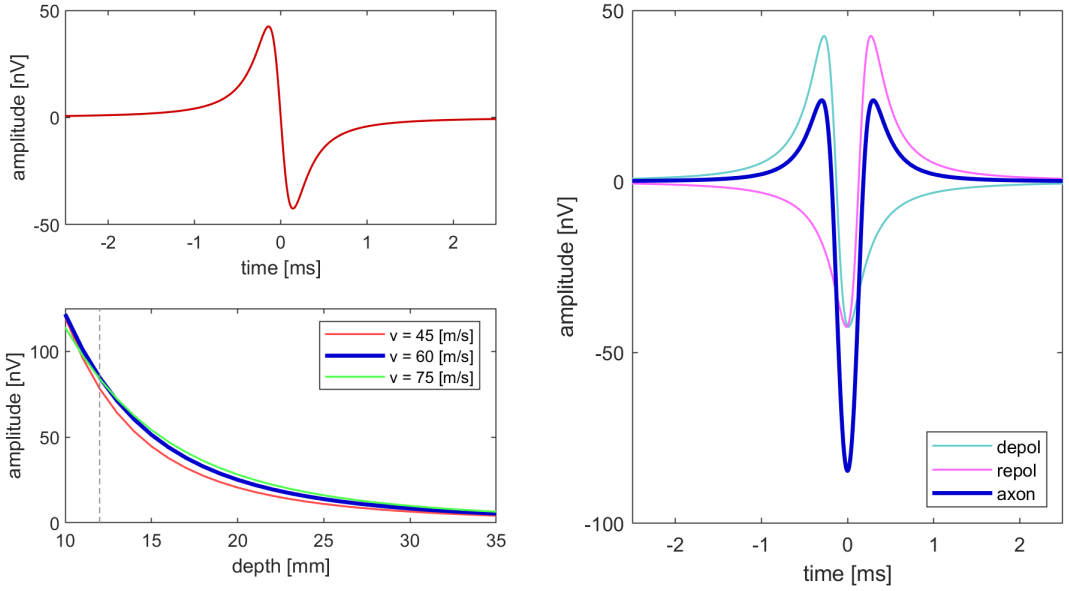

Figure 4: *Top Left:* Moving dipole potential. *Right:* The axon potential (blue) is a superposition of the potentials of the depolarization (cyan) and repolarization (magenta) dipoles. The triphasic morphology of the axon potential reflects the underlying quadrupole source pattern($+--+$). *Bottom Left:* Peak amplitude as a function of depth. The vertical dashed line marks $s = 12\,\text{mm}$. All parameters were taken from Table 1 unless otherwise noted.

at the center of the distributed source. The adjacent small positive deflections are generated by the positive poles at the leading and trailing ends of propagating membrane action potential.

The amplitude of a body surface axon potential is in the order of 100 nV and thus not directly measurable [3].

For the typical depth of a nerve being in the order of several mm or some cm the peak amplitude $\hat{\varphi}_a$ is obtained when setting $t = 0$ (i.e., at the potential minimum). Substituting eq. (1) into (5) we obtain

$$\hat{\varphi}_a = \Delta V_m \frac{\sigma}{\kappa} \frac{A_a v \tau}{\pi \left[v^2\tau^2 + s^2\right]^{\frac{3}{2}}}. \tag{6}$$

The small axonal body surface potentials are caused by the small axonal cross section A_a which is several orders of magnitude smaller than s^2. The bottom left panel in Figure 4 plots $\hat{\varphi}_a$ as a function of s with the parameter v. Noteably, the amplitude decreases quickly with increasing s. As can be taken from eq. (6) for large s peak amplitude is inversly propotional to the third power of s (quadrupole behavior). Thus, eq. (6) supports the choice of clinical recording sites as indicated in Figure 2.

[3] Modern biopotential amplifiers provide resolutions of a few tens of nV at noise levels being in the same order of magnitude. However, the major limiting factor of measuring cellular biopotentials at the body surface is simply the superposition of uncorrelated activity of many cells.

Some Observations: The results obtained in this tutorial are in good qualitative agreement with other studies using more sophisticated modeling ([3] finite element model, [2] membrane potential model). Importantly, all models predict negativity of tissue as a marker for local activation. These model predictions are also in agreement with experimental studies using extracellular micro-electrodes for assessing activity of single axons [4]. These observation does not only apply to neural tissue. Also cardiac muscle tissue becomes negative upon local activation [5]. [4].

2.4. Compound Action Potential

The sensory CAP generated by a large plurality of axons can be obtained by a superposition of all axon signals. However, as illustrated in Figure 5 a) activation in individual axons displays some dispersion. When stimulating a peripheral nerve, a volley is triggered (i.e., a plurality of activation pulses in individual axons). Within this volley, activity is somewhat asynchronous due to variations in stimulation threshold and conduction velocity of individual fibers. In section 2.3 we observed that time shifts can be modeled by a convolution with time-shifted Dirac pulses. Therefore, superposition of axonal potentials may be modeled by summation of many axon potentials dispersed in time. However, for considering the contributions of some hundred axons it is convenient, to define a probability density function $D(t)$ reflecting dispersion of activation (see Figure 5 b) and [2]). The sensory CAP $\varphi_e(t)$ generated by N axons is then obtained by a convolution of the axon potential $\varphi_a(t)$ with the dispersion function $D(t)$

$$\varphi_e(t) = N D(t) * \varphi_a(t). \tag{7}$$

Here, $D(t)$ is defined such, that the area under the curve equals one. The number of axons is considered by multiplication of N.

Probability density distributions may be approximated by histograms (interval width ΔT). We apply the following notation in this tutorial. We chose an odd number of intervals H and center the histogram at $t = 0$. We then obtain $\kappa = {}^{(H-1)}/_{2}$ indices for each negative and positive time shifts. The local densities $d(h)$ must fulfill the following side constrain (area under the curve equals one)

$$\Delta T \sum_{h=-\kappa}^{\kappa} d(h) = 1. \tag{8}$$

Figure 5 b) depicts the example distribution which was chosen in this tutorial. A numerical software package was used for solving equations at a sampling interval of 10 µs. Figure 5 c) depicts the simulated CAP. It displayed a peak amplitude of 2.4 µV. Notably, this value corresponds to roughly the 30-fold of the axonal peal amplitude 85 nV, while the number of axon in the simulation was set to $N = 600$. This remarkable loss of CAP amplitude was due to the asynchronicity of axonal activity (dispersion). As we can observe from Figures 5 b) and c) the convolution of $\varphi_a(t)$ with $D(t)$ may be interpreted as a smearing of axon activity on on the body source. The distribution $D(t)$ remarkably broadens the CAP (superposition of cellular activity) as compared to the axon potential $\varphi_a(t)$ and reduces the increase of amplitude by superposition of N signals.

[4] Cathode stimulation is a frequently used approach. While activated cells generate negativity in their surrounding, negative electrodes activate nearby neurons or myocytes (see also Figure 2).

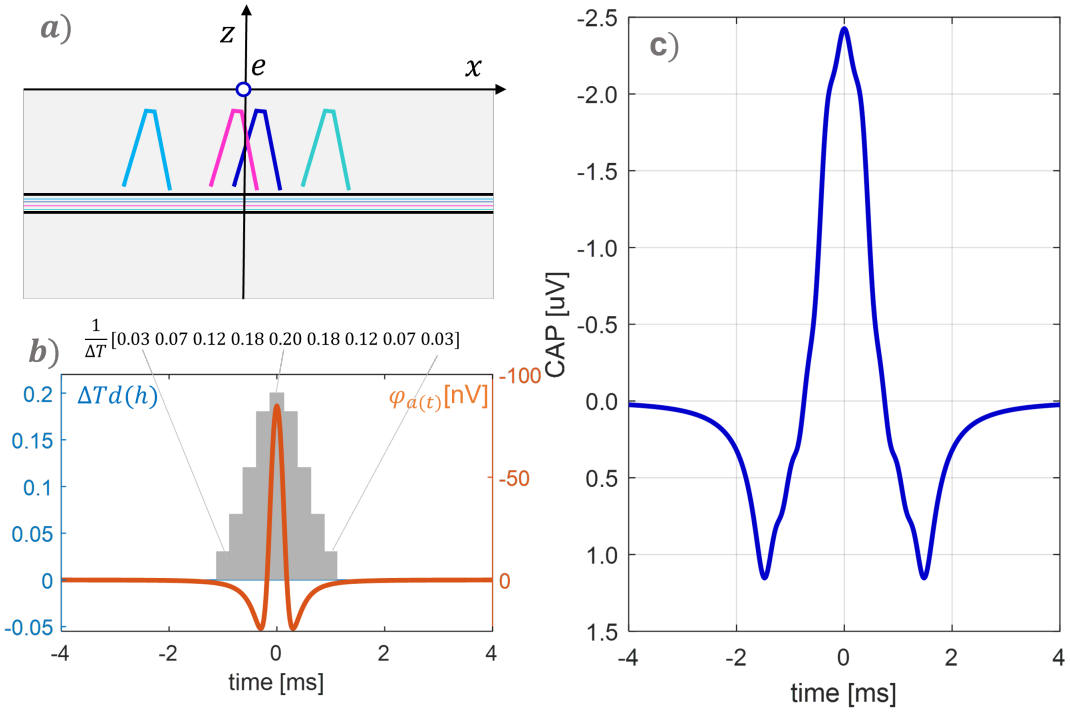

Figure 5: *a)* Schematic representation of four axons in a neural tract displaying a dispersion of activation. *b)* Example for a distribution of dispersion $D(t)$ (gray shaded histogram containing $H = 9$ intervals). On top of this subpanel the used example values are listed. Following the definitions made in eq. (8) the sum of the values inside the square bracket yields one. ΔT was set to 0.3 ms. For comparison, the axon potential $\varphi_a(t)$ is superimposed in the figure at the same time scale (negativity is plotted upwards). *c)* A simulated CAP obtained by numerical convolution of the two functions ($\delta(t)$ and $\varphi_a(t)$) in panel b). Following clinical standards, negativity is plotted upwards (see also text).

The simulated CAP also displays some ripple in the waveform. This ripple was due to the steps in the distribution function $D(t)$. This may be considered as a modeling artifact caused by approximating dispersion by a relatively small number of intervals H. There are multiple options for reducing this artifact. Firstly, the number of intervals H may be increased for decreasing the size of the steps. Secondly, instead of a histogram, a continuous distribution function may be used. Appendix B investigates this second option in more detail.

2.5. Comparison with Measured Data - Erb's Point

For performing an initial validation of the considered CAP-model a comparison with data recorded at erb's point (defined in Figure 2) was performed . In four healthy volunteers right median nerve stimulation was performed and CAPs were recorded at the right erb's point. Following a clinical standard procedure the reference electrode was placed at the left erb's point

and the CAP was obtained by trial averaging of 600 bandpass filtered sweeps [5]. The bandpass corner frequencies were set to 75 Hz to 750 Hz. This choice will be further investigated in Section 3.

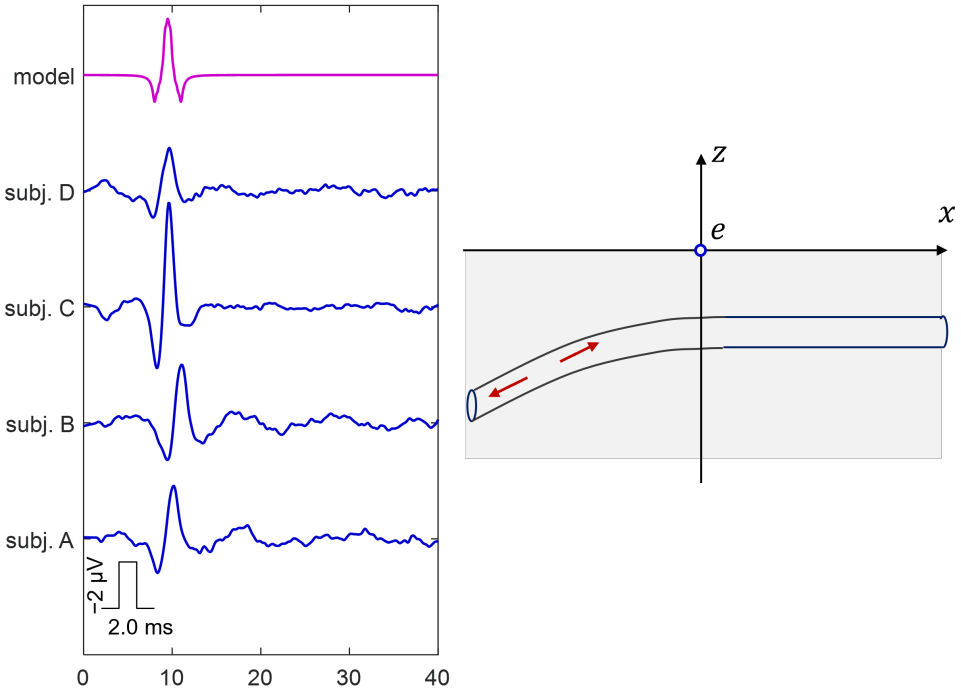

Figure 6: *Left)* Simulated CAP (magenta) and erb-potentials obtained in four normal volunteers (blue traces). The peak of the simulated CAP was located at 9 ms corresponding to the average latency in healthy subjects (N9-peak). In the recorded data a normal variation in amplitude and latency is observable. Here, variations in latency were due to body size (155 to 175 cm) and to a smaller degree due to age (25 to 45 y). For all traces, the width of the negative peak is in the order of roughly 2 ms. In all four subjects the signal morphology is asymmetric. The positivity ahead of the dominating negative peak is more pronounced than the trailing positivity. *Right)* Schematic of the asymmetry of the nerve anatomy near the erb electrode. Due to a curvature in the neural pathway the depolarization dipole is orientated towards the electrode when approaching the recording side generating a larger initial positivity.

The simulated CAP resembles several important features of the recorded CAPs. Amplitude and width are within the experimentally observed range. Furthermore, also the measured signal morphology is dominated by a negative peak with two adjacent smaller positivities. However, in the recorded data the initial positivity is always of larger amplitude. The right panel of Figure

[5]This electrode configuration allows for assessment of conduction velocity of right and left median nerve. For each stimulation site the ipsi-lateral erb-electrode is used as the the active electrode (i.e., for picking up the response to stimulation), while the contra-lateral electrode serves as a reference (potential is almost zero in the far field). Some hundred repetitions are required for extracting the CAP. Notably, the raw signal contains much larger background signals (in particular cardiac signals, i.e., ECGs). Filtering is applied for further improving signal-to-noise ratio.

6 explains the asymmetry of the recorded data by an asymmetry of the underlying geometry. This asymmetry is not considered by the model applied in this tutorial.

Similar traces are obtained we recording median nerve sensory CAPs in the cubital fossa (elbow bend, see [6]) or tibial nerve sensory CAPs in the popliteal fossa (knee bend, see [7]). However, when recording at the extremities the placement of the reference electrode has more impact on the signal morphology, due to the relatively small diameter of essentially cylindrical anatomical structures.

3. Sensory CAP Model – Frequency Domain

The bandpass filtered data in Figure 6 suggest, that sensory CAPs are mainly composed by frequency components in the order of some hundred Hz. For extending our analysis, we insert eq. (4) into eq. (7) and obtain

$$\varphi_e(t) = N\delta(t) * \varphi_p(t) * [\delta(-\tau) - \delta(-\tau)]. \tag{9}$$

This time domain CAP representation involves two convolutions. Convolutions in the time domain correspond to multiplications in the frequency domain. This eases frequency domain analysis, since the model can be split into independent blocks. For each block time continuous Fourier transform can be applied independently. The spectrum of the entire system is then obtained by multiplying the spectral representations of each block. Thus, the frequency domain analysis contains tree blocks:

- The source term on cellular level (single axon) is modeled by two Dirac pulses representing de- and repolarization.
- The potential $\varphi_p(t)$ related to propagation of a dipole along a fiber composes a second block.
- The dispersion of activity $\delta(t)$ is modeled by a third block.

We restrict our investigations to a frequency range below 1 kHz. As it is shown in [1] the quasi-stationary dipole model introduced in section 2.3 applies to that low frequency band. At some kHz and above, cell membranes behave like capacitors short-cutting the signal.

3.1. Source Term

The Fourier transform of two Dirac pulses of opposite sign can be denoted by

$$\mathscr{F}\{\delta(-\tau) - \delta(-\tau)\} = e^{-j\omega\tau} - e^{-j\omega\tau} = -2j\sin(\omega\tau). \tag{10}$$

Thus, the magnitude of the spectral source term can be approximated by a sine. For $\tau = 0.13$ ms (see Table 1) its first maximum is obtained at 1.9 kHz. Thus, in the frequency range of interest the source block behaves like a high-pass structure. Figure 7 illustrates this observation [6].

[6] Due to the relatively short membrane potential duration being in the order of some tenth of ms, the coarse approximation of the biphasic current by two Dirac pulses provides sufficient accuracy below 1 kHz. A more detailed model of a peripheral mammalian sensory fiber is investigated in [2]. Figure 4 in this open access paper depicts the results. There is a remarkable agreement with the simplified treatment in this tutorial.

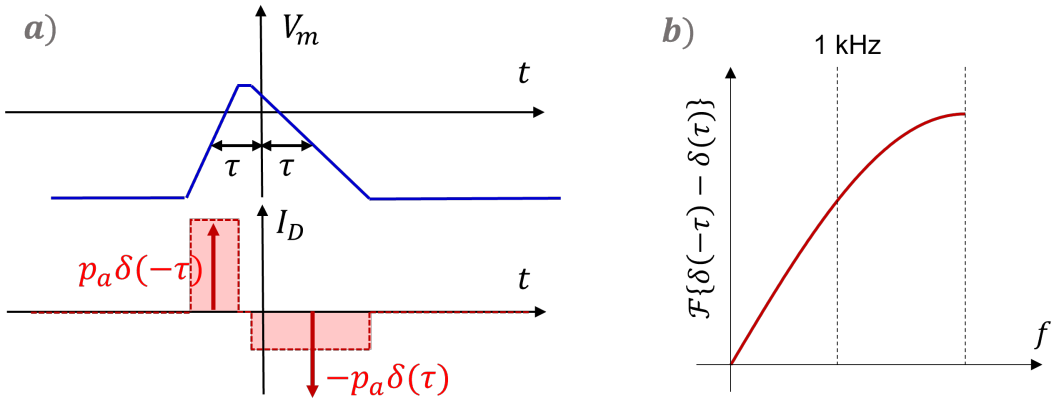

Figure 7: *a)* A piece-wise linear model of the membrane potential $V_m(t)$ and the impressed current $I_D(t)$ related to the first temporal derivative of V_m. The current displays a biphasic pattern. Importantly, the areas under each half wave (reddish style) are identical. Therefore, they are approximated by two Dirac pulses of identical amplitude but opposite sign. *b)* The spectrum of the biphasic wave displays a peak well above 1 kHz. In the relevant frequency range the source term displays high-pass properties.

3.2. Propagation Term

The propagation term is defined in eq. (3). However, despite its closed form the analytical computation of its Fourier transform it is not straight forward but significant spectral properties can be observed by analysising formulas. Since the propagation term is an odd function (see top left panel of Figure 4), its DC-content equals zero. Furthermore, since it is a continuous finite valued function, its spectral components approach zero when increasing frequency towards infinity. Therefore, dipole propagation acts like a band-pass.

Furthermore, a numerical investigation of the spectrum can be performed. At the high sampling rate of 100 kHz accurate spectral estimates are obtained up to serveral kHz. Figure 8 depicts the results.

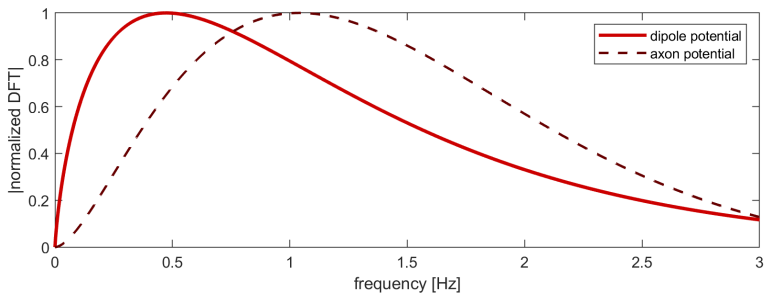

Figure 8: Frequency spectrum of the signal generated by a propagating dipole (bold line). For the parameters defined in Table 1 a peak frequency of approximately 500 Hz is obtained. The dash line depicts the spectrum of an axonal potential $\varphi_a(t)$. It is the product of the bold line with the high-pass structure in Figure 7. Here, the maximum is shifted up to about 1 kHz.

3.3. Dispersion Term

Figure 9 depicts the concept used for frequency domain analysis of the distribution function $D(t)$ as defined in eq. (8). The histogram $D(t)$ may be interpreted as a convolution of a series of Dirac pulses $f_\delta(t)$containing the amplitudes of each bar in the histogram and rectangular pulse $f_r(t)$ of width ΔT and amplitude one

$$D(t) = \frac{1}{\Delta T} f_\delta(t) * f_r(t) = \frac{1}{\Delta T} \sum_{h=-\kappa}^{\kappa} d(h)\delta(t + h\Delta T) * f_r(t) \tag{11}$$

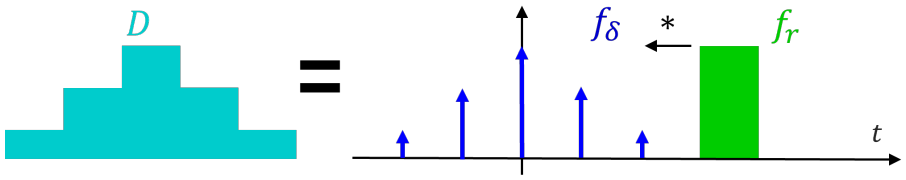

Figure 9: A histogram $D(t)$ (left) can be interpreted as the convolution of a series of Dirac pulses $f_\delta(t)$ sampling the interval amplitudes (middle) with a rectangular pulse $f_r(t)$ (right).

In this tutorial we first consider the special case that the distribution $D(t)$ was even (i.e., $d(-h) = d(h)$). We then obtain for the Fourier transform of $f_\delta(t)$

$$\mathscr{F}\{f_\delta(t)\} = d(0) + 2\sum_{h=1}^{\kappa} d(h)\cos(h\omega\Delta T) \text{ ... for } d(-h) = d(h). \tag{12}$$

Thus, the series of Dirac pulses displays a periodic spectrum[7]. Due to the even distributions it contains only cosine terms. At $\omega = 0$ all cosine terms yield one. In statistical distributions the parameters $d(h)$ are always positive numbers and their sum yields one. Thus, we obtain a spectral maximum at DC and the value of this maximum equals one. Due to the periodicity of the spectrum there are multiple maxima which all equal one.

The Fourier transform of the rectangular pulse $f_r(t)$ is well described in basic literature [8]. It is represented by a sinc-function

$$\mathscr{F}\{f_r(t)\} = \sqrt{\frac{2}{\pi}}\frac{\sin(\omega\Delta T)}{\omega}. \tag{13}$$

Notably, the sinc-function contains a single global maximum at $\omega = 0$. Due to the time domain convolution in eq. (11) its Fourier transform is obtained by multiplying eq.s (12) and (13)

$$\mathscr{F}\{D(t)\} = \mathscr{F}\{f_\delta(t)\}\,\mathscr{F}\{f_r(t)\}. \tag{14}$$

Figure 10 shows the spectrum obtained by eq. (15) for the parameters chosen in this study. At $\omega = 0$ the maxima in $\mathscr{F}\{f_\delta(t)\}$ and $\mathscr{F}\{f_r(t)\}$ coincide. At non-zero frequencies the maxima in the periodic spectrum $\mathscr{F}\{f_\delta(t)\}$ coincide with the zero-crossings in the sinc-function

[7]We may interpret the series of Dirac pulses as time discrete sampling of the histogram. Thus, following Shannon's sampling theorem a periodic spectrum is obtained,

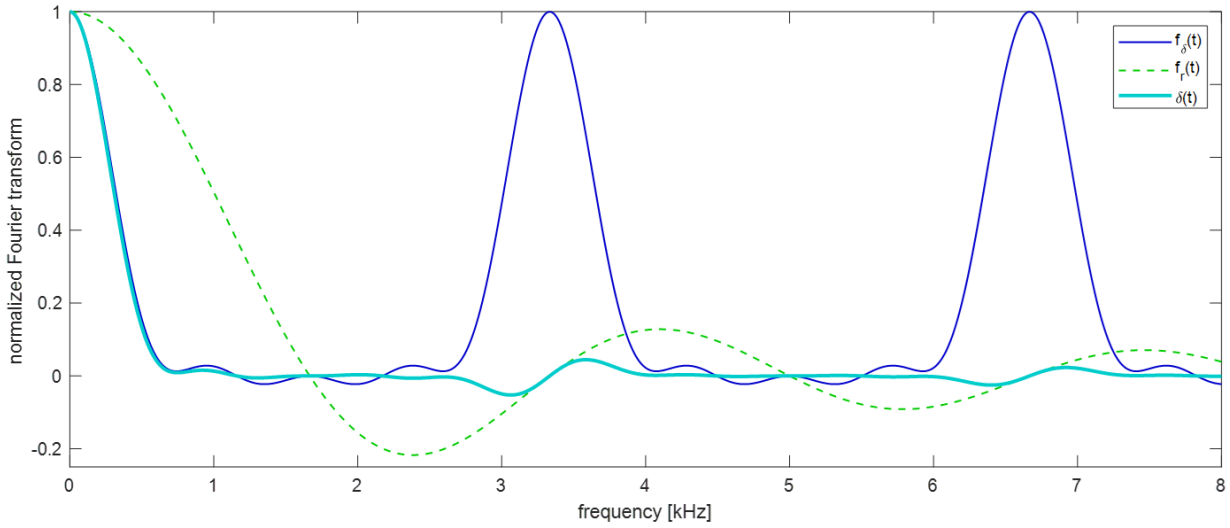

Figure 10: The series of Dirac pulses $f_\delta(t)$ yields a periodic spectrum (blue trace). The spectrum of the rectangular pulse $f_r(t)$ is a sinc-function (green dashed trace). Due to the convolution depicted in Figure 9 the spectrum of the distribution function is the product of its two components. The amplitude of the spectra was normalized to one for enabling comparison. Parameters were selected identical as for the time domain investigation in Figure 5.

in $\mathscr{F}\{f_r(t)\}$. Therefore, we obtain a single global maxium in the spectrum of the distrbution function $\mathscr{F}\{D(t)\}$. Furthermore, with increasing ω the envelope of the sinc-function decreases by $1/\omega$. Thus, the spectrum of $\mathscr{F}\{D(t)\}$ corresponds to a low-pass. In the stop-band the cosine and sine terms induce some ripple in the spectrum. The $1/\omega$ damps this residual ripple with increasing frequency. Analogues as for the time domain (see Figure 5) this ripple is due to the steps in the histogram.

Harmonic Functions: In this section we restricted our analysis to modeling statistic distributions by even histograms. However, there is a more general body of theory available which allows us to generalize the observations made in this section to both asymmetric and also smooth statistical distributions[8]. Statistic distributions have two remarkable properties which allow for generalization. They contain only positive numbers and the area under the curve always equals one. The term harmonic functions refers to Fourier analysis of functions fulfilling these two criteria (mind the cosine and sine terms in our analysis). The Fourier transform of statistic distributions always displays the global maximum at $\omega = 0$ and always converges towards zero when ω approaches infinity. Thus, temporal dispersion always acts as a low-pass filter. The supplement of [2] provides an open source document containing additional information on harmonic functions.

[8]If we would apply a bell shaped Gaussian distribution instead of the even histogram, we would obtain a bell shaped spectral distribution with the maximum at $\omega = 0$. Notably, the result for $\mathscr{F}\{D(t)\}$ in Figure 10 can be interpreted as an approximation of a bell-curve.

3.4. CAP Frequency Spectrum

Applying Fourier transform to eq. (9) the spectrum of a sensory CAP is obtained by the product of the three components described above

$$\mathscr{F}\{\varphi_e(t)\} = N\mathscr{F}\{D(t)\}\,\mathscr{F}\{\varphi_e(t)\}\,\mathscr{F}\left\{\delta_(t-\tau) - \delta_(t+\tau)\right\}. \tag{15}$$

Here, the source term $\mathscr{F}\left\{\delta_(t-\tau) - \delta_(t+\tau)\right\}$ corresponds to a high-pass component and the distribution term $\mathscr{F}\{D(t)\}$ corresponds to a low-pass component. Thus, their product is a band-pass. Also the propagation term $\mathscr{F}\{\varphi_e(t)\}$ relates to a band-pass. Therefore, the dominating spectral components of a sensory CAP are contained within a spectral band. Figure 11 depicts the frequency spectrum obtained for the sensory CAP in Figure 5.

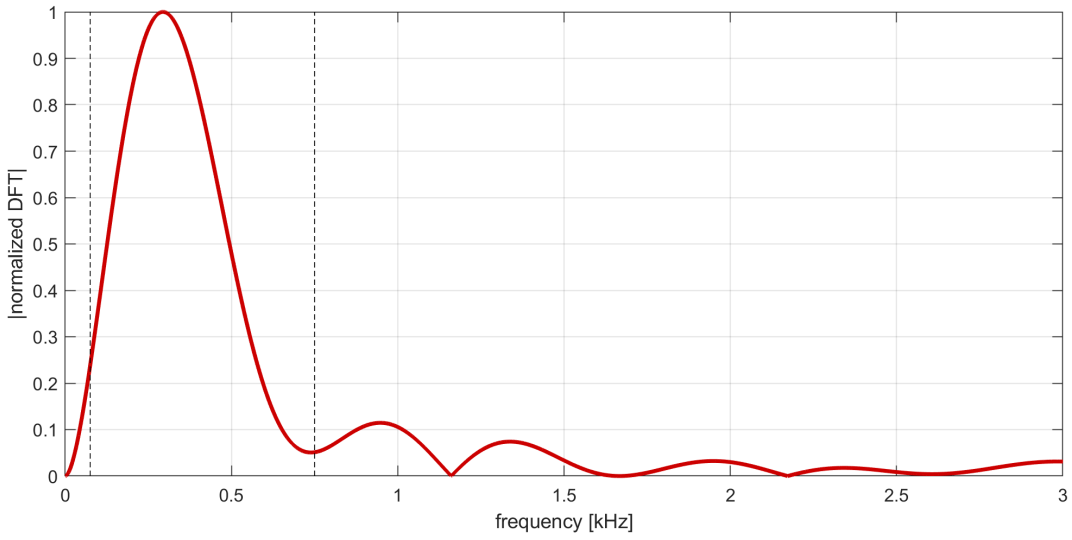

Figure 11: Normalized magnitude of the Frequency spectrum for the sensory CAP in 5. The dashed lines are the corner frequencies which were applied to the experimental data in Figure 6 (depicted for comparison; 75 Hz and 750 Hz). Also the dominating spectral components of the simulated CAP are within this band.

Again, some ripple occurs at high frequencies due to the application of a step-like distribution function. In Appendix B it is shown that a continuous distribution function significantly reduces these spurious oscillations for both the time and the frequency domain.

Experimental validation of the sensory CAPs spectrum is challenging since real world data displays a superposition of the target signal with background signals (for example mypotentials) of high amplitude. Appendix C provides a spectral analysis of an Erb potential. Similar as for the simulated data peaj frequency was found near 200 Hz and bandwidth was some 100 Hz.

4. Observations and Interpretations

4.1. Model Definition

The art of modeling: *"Every model is a simplification of reality and the development described here is no exception."* This first sentence quoted from the discussion in Blanc et al. [9]

applies to any modeling approach. Models are per definition simplified or abstract reflections of reality. There is nothing bad in this phrase – indeed, it teaches how to use models. Any phenomenon we observe in the true world is influenced by a large plurality of effects. Human perception in general uses abstraction. We always work with simplified pictures of what is going on around us. Modeling is the art of making a conscious approach of simplification: consider an abstract picture and understand the most important effects; refine the picture if needed in a step-like fashion by considering more and more single factors contributing to the reality around us.

Since models are always approximations and never perfect copies of reality, it is mandatory to define a scope for each model. For this tutorial it may be defined as follows:

Scope: Describe the genesis of a basic neuropotential by a model which requires only a few dipole terms in closed form. Apply this model for explaining the key properties of the signal in the time and frequency domain in a hopefully transparent way.

Interpretation: Sensory CAPs were chosen, since they allow for meeting this scope and for explaining the remarkable changes of signal properties on their way from the cell membrane to the body surface (Figure **??**). The applied model allowed for explaining body surface potentials as a superposition of cellular de- and repolarization, each described by dipoles. Dipole orientation explains negativity of activated tissue. A plurality of effects contribute to explaining the low amplitude of body surface potentials. Firstly, the cross-section of the activated intra-cellular space (impressed currents) is small compared to the cross-sections available for passive current return path. Therefore, potential gradients are relatively small close to the body surface. Secondly, de- and repolarization display opposite sign compensating each other in the far field. Finally, individual cells get activated in a slightly asynchronous fashion resulting in a smearing of signal peaks.

The model allowed for identifying three effects contributing to the spectral profile of the body surface signal – and, thus, providing a theoretical basic for improving signal extraction by filters. Firstly, the fast de- and repolarization cycle at the cell membrane constitutes a source containing significant high frequency components. Secondly, propagation of activation along an axon acts like a band-pass filter in signal transmission. Finally, smearing due to dispersion of activation acts as a low-pass filter and strongly damps the high frequency components in the source term.

Some obvious simplifications: The choice of a half-space model which allows for application of closed expressions hampers modeling of anatomical structures and introduces an idealized symmetry which does not reflect real word conditions. The application of numerical field computation techniques can overcome this limitations. Models may describe human anatomy and

may consider structures of different conductivities (e.g., bones, muscles). The approximation of the source structure by two dipoles does not allow for accurate modeling of the action potential and detailed features like hyperpolarization are not contained in the models. A technique for overcoming these shortcomings is presented in [2].

It is an intrinsic challenge of scientific working aiming to overcome obvious limitations. This tutorial is intended for motivating future researchers to do so.

4.2. Uncertainty of Model Parameters

Assigning values to model parameters always involves some uncertainty. When modeling biological systems this uncertainty in general larger as for technical systems. When considering the individual variation in Figure 6 it becomes evident that there is some individual variation in these parameters. The following approach was made in this tutorial. Reasonable values were assigned to the parameters based on data reported in literature. The uncertainty in conductivities and axon cross section might be in the order of a few tens of percent. Uncertainty in membrane potential amplitude might be even smaller. Notably, all parameters mentioned in this paragraph contribute only to a scaling of the signal. Thus, they cannot get estimated independently from the recorded data.

Reliable data for the number N of axons in a volley and their temporal dispersion is hard to obtain. Thus this data was selected (fitted) such that the simulated signal is comparable to the measured data in amplitude and width. The selected value of 600 axons corresponds to a total cross section of $0.06\,\mathrm{mm}^2$ for the stimulated axons which appears reasonable. The temporal dispersion in the volley is in the order of slightly more than $\pm 10\,\%$ of the conduction time from the stimulation site to the recording site (9 ms) on average from the wrist to erb's point). Also this appears being a plausible value.

5. Summary and Outlook

The half-space model provides a reasonable approximation for explaining key signal properties of sensory CAPs. In the frequency domain, three effects contribute to the spectral profile (see Figure 12). The biophysical properties of the pulse-conducting axons directly impact on signal morphology and amplitude. Since axons display a higher conduction velocity and shorter action potential duration as most other cell types, sensory CAPs contain relatively high frequencies. Spectral amplitude peaks at some hundred Hz and significant activities occurs up to about 1 kHz[9].

Other types of biopotentials like the electroenzephalogramm (EEG), and the electrocardiogramm (ECG) and are generated by comparable effects as described in this tutorial. However, an obliviously broader spectrum of biophysical effects must by considered. Here, a brief outlook is provided in the context of Figure 12.

Source: In by far the most of the cases the action potential duration is significantly longer as compared for the axon. This generates source terms of much smaller frequency content which contributes to spectral peaks of smaller frequency for the EEG and the ECG. In the human

[9] Generally, 1 kHz reflects a kind of upper bound of body surface spectral components.

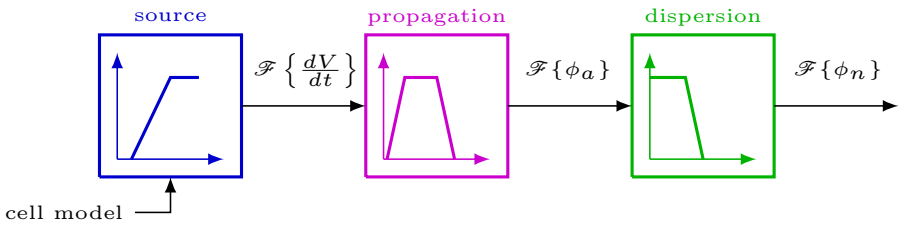

Figure 12: Overview on the frequency domain structure considered in Section 3. The source term (impressed current) is obtained from the first derivative of the membrane action potential (cell model). In the relevant frequency range, the source term reflects high-pass structure. The propagation along an individual axon behaves like a band-pass structure. Temporal dispersion of individual cells behaves like a low-pass structure.

cortex the neuron's dendrites (action potential duration of several ms) are the dominating structure of EEG generation while axonal signal components are expected to be much smaller amplitude [10] . In the human heart action potential duration is in the order of a few 100 ms. Thus distinctly separated deflections for depolarization (QRS-complex) and repolarization (T-wave) are observed. Interestingly, within the ventricles of the human heart, cells display a natural heterogeneity of action potential duration which essentially reverses the direction of propagation during repolarization. Therefore, the two dominant ECG-deflections, R- and T-wave, both display a positive sign and the ECG contains a natural DC-content [11].

Propagation: Large EEG waves like for example the α-rhythm (8 to 13 Hz) are generated by propagation of activation across large macroscopic areas of brain tissue. Here, neurons transmit activation to neighboring cells via synapses. This causes a slowing of conduction by more than an order of magnitude (as compared to the axon) and involves denditric activity. Both effects contribute to a reduction of peak frequency. In the heart myocytes transmit activation via gap junctions. Conduction velocities are in the order of roughly $1\,\mathrm{m\,s^{-1}}$ and, thus, again more than an order of magnitude smaller as for the myelinated axon. Propagation of activation fronts in the ventricles generate the QRS-complex and, thus, the fastest deflections in the normal ECG [1].

Dispersion: In the EEG the low-pass effect of asynchronous activation is supposed to strongly attenuate axonal activity (short AP duration) while having much less on effect on dendritic activity. Thus, within the classical EEG spectral bands (Δ-band to γ-band; 4 to 70 Hz, [12]) dispersion might largely mask cortical axonal activity. However, for the highest spectral peaks measurable on the scalp (near 600 Hz; [13]) a high degree of neuronal synchronization may occur. This gives rise to fast low amplitude oscillations of some 100 nV peak-to-peak voltage. In the human heart significant dispersion of repolarization is observable [14]. Thus, T-waves are of smaller amplitude and smoother shape (lower frequency) as compared to the QRS complex.

Revision History

v1.0.a October 22, 2024, creation
v1.0.b October 28, 2024, add affiliation, update Figure 2

References

[1] J. Malmivuo, R. Plonsey, Bioelectromagnetism - Principles and Applications of Bioelectric and Biomagnetic Fields, Oxford University Press, New York, 1995.
URL https://www.bem.fi/book/

[2] G. Fischer, M. Kofler, M. Handler, D. Baumgarten, A Lead Field Two-Domain Model for Longitudinal Neural Tracts – Analytical Framework and Implications for Signal Bandwidth, Comput Math Methods Med 2020 (2020) 5436807. doi:https://doi.org/10.1155/2020/5436807.

[3] J. Clark, R. Plonsey, The extracellular potential field of the single active nerve fiber in a volume conductor, Biophys. J. 8 (7) (1968) 842–864.

[4] C. H. Chen, E. A. McCullagh, S. H. Pun, P. U. Mak, M. I. Vai, P. I. Mak, A. Klug, T. C. Lei, An integrated circuit for simultaneous extracellular electrophysiology recording and optogenetic neural manipulation, IEEE Transactions on Biomedical Engineering 64 (3) (2017) 557–568. doi:10.1109/TBME.2016.2609412.

[5] G. Fischer, B. Tilg, R. Modre, G. Huiskamp, J. Fetzer, W. Rucker, P. Wach, A bidomain model based bem-fem coupling formulation for anisotropic cardiac tissue., Annals of Biomedical Engineering (2000). doi:10.1114/1.1318927.

[6] D. MacDonald, Z. Al-Zayed, B. Stigsby, I. Al-Homoud, Median somatosensory evoked potential intraoperative monitoring: Recommendations based on signal-to-noise ratio analysis, Clinical Neurophysiology 120 (2) (2009) 315–328. doi:https://doi.org/10.1016/j.clinph.2008.10.154.
URL https://www.sciencedirect.com/science/article/pii/S1388245708012388

[7] T. Sand, M. B. Kvaly, T. Wader, H. Hovdal, Evoked potential tests in clinical diagnosis, Tidsskr. Nor. Laegeforen. 133 (9) (2013) 960–965.

[8] E. Kreyszig, Mathematical physics, Engineering mathematics, eighth Edition, John Wiley & Sons, New York, 2008.

[9] O. Blanc, N. Virag, J.-M. Vesin, L. Kappenberger, A computer model of human atria with reasonable computation load and realistic anatomical properties, IEEE Transactions on Biomedical Engineering 48 (11) (2001) 1229–1237. doi:10.1109/10.959315.

[10] T. R. Knösche, J. Haueisen, EEG/MEG Source Reconstruction, 1st Edition, Springer, 2022.

[11] G.-X. Yan, C. Antzelevitch, Cellular basis for the normal t wave and the electrocardiographic manifestations of the long-qt syndrome, Circulation 98 (18) (1998) 1928–1936. doi:10.1161/01.CIR.98.18.1928.

[12] G. Fischer, J. Haueisen, D. Baumgarten, M. Kofler, Spectral separation of evoked and spontaneous cortical activity, part 1: Delta to high gamma band, Biomedical Signal Processing and Control 92 (2024) 106094. doi:https://doi.org/10.1016/j.bspc.2024.106094.

[13] G. Fischer, J. Haueisen, D. Baumgarten, M. Kofler, Spectral separation of evoked and spontaneous cortical activity, part 2: Somatosensory high frequency oscillations, Biomedical Signal Processing and Control 95 (2024) 106456. doi:https://doi.org/10.1016/j.bspc.2024.106456.

[14] M. S. Fuller, G. Sándor, B. Punske, B. Taccardi, R. S. MacLeod, P. R. Ershler, L. S. Green, R. L. Lux, Estimates of repolarization dispersion from electrocardiographic measurements, Circulation 102 (6) (2000) 685–691. doi:10.1161/01.CIR.102.6.685.

[15] R. Sauerheber, B. Heinz, Temperature effects on conductivity of seawater and physiologic saline, mechanism and significance, Chemical Sciences Journal 6 (4) (2015) 109.

Appendices

A. Model Parameters

This section motivates the choice of parameter values used in this tutorial.

Membrane Potential Amplitude ΔV_m: This value is typically in the order of 100 mV which somewhat below the difference of the sodium and pottassium potentials at the cell membrane. For example the amplitude obtained from a Hodgkin-Huxley model in the textbook by Malmivuo and Plonsey ([1], Figure 4.19) is slightly below this value while the amplitude obtained for a model of a mammalian cell [2] is slightly above this value.

Effective Intracellular Conductivity σ: This value essentially reflects the ohmic conduction of an aqueous saline solution. At body temperature the conductivity of a physiological saline solution is approximately $2\,\mathrm{S\,m^{-1}}$ [15]. Some studies report slightly smaller values [2] since organelles inside the cells reduce the effectively conduction cross-section.

Bulk Conductivity κ: This value reflects the ohmic conduction of tissue being a mixture of many components. There is some obvious variability. Highest, conductivity is observed in blood (approximately $0.6\,\mathrm{S\,m^{-1}}$). This value is about on third of the conductivity of a physiological saline solution. Here, the hematocrit inside the blood reduces conductivity since at low frequencies passive current flow propagates essentially in the extracellular space only. Lowest conductivity is observed in bone or lung tissue (contains air) and amounts to about $0.05\,\mathrm{S\,m^{-1}}$). Average tissue conductivity is in the order of $0.2\,\mathrm{S\,m^{-1}}$) which is also a reasonable approximation for most soft tissues.

Nerve Conduction Velocity v: A typical value for myelinated nerve fibers in humans and mammalians is in the order of 60 m s. This value is the mean of a larger range which was investigated in [2].

Action Potential Time Constant τ: As can be taken from Figure 3 τ is defined such that it equals approximately one quarter of the time from activation onset to repolarization end (i.e., transition to hyperpolarization). The simulated membrane potential in [2] this time interval is somewhat above 0.5 ms suggesting a value of τ =0.13 ms.

Number of Axons N: There is quite a large uncertainty when reviewing literature for estimates of firing neurons. For example, Section 2.4.2.1 of the textbook by Knösche & Haueisen [10] reports values from a few thousand up to several ten-thousand when estimating the number of active cortical neurons generating measurable scalp potentials. This tutorial chose a value of $N = 600$ (about on third of the value reported in [2]) since this choice provided a peak amplitude which was comparable to the experimental data. The estimation of the activated cross-section within a nerve (see Section 4.2) delivered a plausible value.

Depth s: This value was based on an estimation made by clinical neurophysiologists based their clinical experience.

B. Continuous Distribution

The rectangular steps in the histogram used in the tutorial generated spurious high frequency components in the sensory CAP. This Appendix illustrates the attenuation of this modeling artifact by applying a continuous statistical distribution.

In section 3.4 the histogram $D(t)$ was modeled as a convolution of a series of Dirac pulses $f_\delta(t)$ with a rectangular pulse $f_r(t)$ of width ΔT and amplitude one. By performing a second convolution with a rectangular pulse $\bar{f}_r(t)$ the step-like histogram gets converted into a continuous, piece-wise linear distribution function $\tilde{D}(t)$ (convolution of two rectangles generates a continuous triangular pulse). Here, the pulse $\bar{f}_r(t)$ was normalized such that its area yields one. We obtain

$$\tilde{D}(t) = \frac{1}{\Delta T} f_\delta(t) * f_r(t) * \bar{f}_r(t) \tag{16}$$

Figure 11 depicts the CAP obtained by using the continuous distribution function $\tilde{D}(t)$. Figure 12 depicts the Fourier transform tor the CAPs obtained from both distributions.

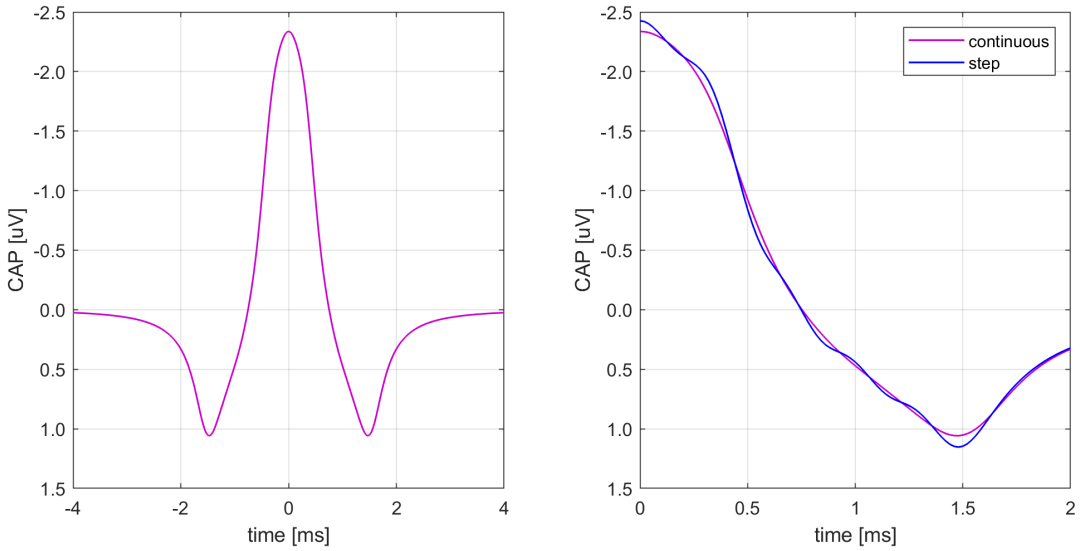

Figure 11: *Left)* CAP obtained by using the continuous distribution function $\tilde{D}(t)$. A smooth triphasic morphology is obtained. *Right)* Comparison of CAP obtained from $\tilde{D}(t)$ (magenta) and the histogram $D(t)$ (blue). A portion of the signal was magnified for illustrating attenuation of oscillations by double convolution.

C. Spectral Analysis of an Erb's Point Signal

A direct experimental validation of the CAP spectrum is challenging, since in real world recordings the evoked sensory CAP is superimposed by much larger background activity. The top left panel in Figure 13 shows that electrocardigraphic background activity dominates the measured raw data in erb's point recordings. Following clinical practice bipolar recordings were performed by placing electrodes on the right and left erb's point.The bottom right panel displays the sensory CAP extracted by trial averaging and filtering. The deflection is of much smaller amplitude and much shorter duration than the ECG waves in the background.

N-Interval Fourier Transform Analysis (N-FTA) allows for spectral separation of spontaneous background activity and triggered evoked signal components [12]. Spectral components are reflected by power spectral density (PSD, in dB)[10]. While background activity is assessed continuously, evoked

[10]The computation of dB values requires the choice of a reference power level. According to the definitions made in [12] 0 dB correspont to a reference power level of $\mu V^2\,Hz^{-1}$ which is a reasonable choice for EEG

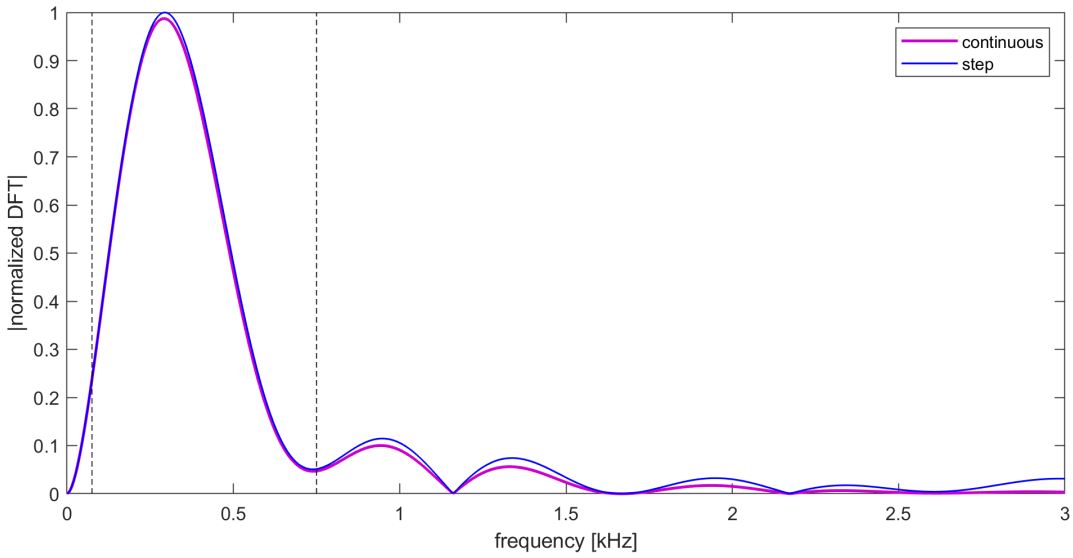

Figure 12: Normalized DFT of the CAPs obtained from $\tilde{D}(t)$ (magenta) and the histogram $D(t)$ (blue). Smoothing by double convolution strongly attenuates frequencies in the range of some kHz.

activity must fulfill statistical acceptance criteria for ensuring that they can be reliably extracted from the data. The right panel in Figure 13 depicts an N-FTA analysis performed for five minutes of data (approximately 750 sweeps). Over the entire investigated frequency range (DC to 1 kHz) the background PSD clearly exceeds the evoked PSD. Evoked components are detected between about 100 Hz and 750 Hz. For the actual sweep count, N-FTA can theoretically detect evoked components down to $10 \log_1 0(750) = 29$ dB below the background value. The peak of the evoked PSD is near 200 Hz and approximately 15 dB below the background PSD. Thus, the experimentally observed spectral distribution agrees with the theoretical prediction in Figure 11.

Notably, there is a defined segment were the evoked activity is less than 29 dB below the background. Only within this segment evoked signal components can be extracted. For improving signal-to-noise ratio, frequencies below, e.g., 75 Hz should be removed by a high-pass filter for excluding the high amplitude ECG-low frequency components from the analysis. Note, that the short CAP duration allows for distinguishing this signal from significant ECG components. For damping also the high frequency noise floor a 750 Hz high-pass filter should be applied.

data.

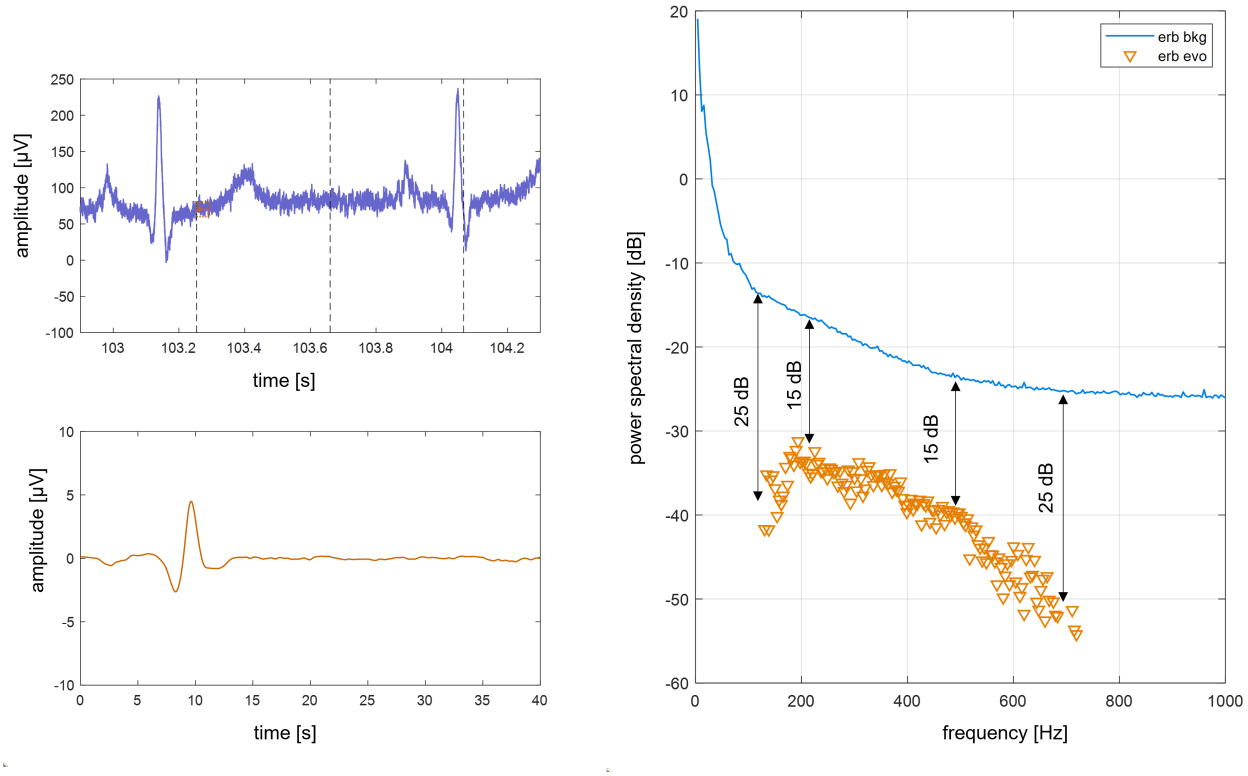

Figure 13: *Top Left:* A 1.4 s segment of data recorded between the right and left erb's point in a volunteer during right median nerve stimulation. The vertical dashed lines mark the stimulation triggers (approximately 2.5 Hz). The stimulation artifacts were removed from this data by template subtraction. This preprocessed data reflects an ECG (a signal measured at the shoulders corresponds to Einthoven lead I). A small orange inset shows the size of the CAP for comparison. *Bottom Left:* The CAP as obtained by trail averaging and filtering (data for subject C in Figure 6). For both time and amplitude significantly smaller scales are used as for the raw data. *Right:* Spectral analysis by N-FTA allows for separation of spontaneous activity (background) and evoked activity in the spectral domain (see text).